Characterization of Rodent Heterotopic Heart Transplantation Models with Cellular and Functional MRI

Q. Ye[1], Y. L. Wu[1], B. D. Barbe[1], F-C. Yeh[1], L. Liu[1], L. M. Foley[1], T. K. Hitchens[1], and C. Ho[1]
[1]Pittsburgh NMR Center for Biomedical Research, Carnegie Mellon University, Pittsburgh, PA, United States

INTRODUCTION: Heterotopic heart or heart-lung transplantation models are pivotal in transplantation research. Depending on vessel configurations and the graft location, the models might expect to have different myocardium morphogenesis and lymphangiogenesis, yet pressure and volume loading of the graft hearts may vary greatly. The rejection or functional status of the graft hearts are usually determined by palpation or ECG in majority of cases (1). However, complementary tests might add some relevant information when assessing effects of immunosuppressive therapy and surgical procedure. The unreliable assessment can have a major impact on the interpretation of experiment results. Cardiac MRI has the advantages of providing very high spatial and temporal resolution along with excellent soft tissue contrast for non-invasively characterization of detailed cardiac anatomy and function with real-time and whole graft information (2). The aim of this study is to characterize the rejection states and cardiac function of two different types (working and non-working heart) heterotopic transplantation models by cellular and functional MRI, to evaluate which model is better for studying the allograft rejection by MRI, and whether palpation or ECG are adequate in assessing graft conditions.

METHODS: Two types of rodent heterotopic heart transplantation models were adapted for this study using Lewis-to-Fisher344 rats: a working heart model with heart and lung and a non-working heart model with heart only. For the working heart model, an en bloc of heart and lung was placed in the receipt abdomen with graft aorta and superior vena cava (SVC) anastomosed with recipient abdominal aorta and inferior vena cava (IVC), respectively. The natural configuration of pulmonary and coronary circulation is preserved; the graft heart receives sufficient volume and pressure loading and exhibits wall motion close to native hearts. For the non-working heart model, the graft aorta and pulmonary artery was anastomosed in an end-to-side fashion to the recipient abdominal aorta and IVC respectively. The major limitation of the model is the lack of what is known as 'volume loading' of the left ventricle (LV). Global cardiac function was evaluated with cine MRI and the regional wall motion and strains were evaluated with tagging MRI followed by strain analysis. For cellular MRI, micro-meter sized iron oxide (MPIO) particles were used to label immune cells, especially macrophages, *in vivo*. The infiltration of labeled macrophage in the rejecting grafts were tracked with *in vivo* T_2^*-weighted imaging, and confirmed with *ex vivo* MR microscopy at 11.7 Tesla. The graft rejection status was evaluated by pathology.

RESULTS: Two weeks after transplantation surgery, graft hearts with both models had strong palpation when touching and both showed normal ECG profiles. However, cine MRI (Fig. 1 A to D) revealed that the graft hearts from the non-working heart model had very poor global cardiac function compared to those from the working heart model. At post-operational-day (POD) 7, the non-working heart model had only less than half of the left-ventricular (LV) blood volumes (LVED and LVES) and stroke volumes (SV) than the working heart model, although having similar ejection fraction (EF). By POD 14, SV of the non-working heart grafts has diminished to almost zero, whereas the grafts from the working heart model preserved the same or better global cardiac functions. Tagging MRI followed by strain analysis (Fig. 1 E & F and Fig. 2) is used to evaluate regional LV wall motions. The non-working heart graft showed almost none circumferential strains (Fig. 1E, Fig. 2A&B) and very little radial strains (Fig. 1F, Fig. 2 E) at POD 7, which almost diminished completely by POD 14 (Fig. 1F, Fig. 2 F). On the contrary, the transplant heart from the working heart model exhibited fair wall motion and strains (Fig. 1 E & F and Fig. 2, C & G), which improved at POD 14, as the grafts recovered further from the transplantation surgery, even though the allograft rejection has progressed further. Immune cells, especially macrophages, infiltrated to the allograft hearts due to rejection can be detected with MRI by labeling with MPIO particles. *Ex vivo* MR microscopy (MRM) (Fig.3) revealed that the non-working heart graft has much more immune cell infiltration compared to the working heart model. This indicates that the non-working heart graft rejects much faster and earlier than the heart-lung working-heart model.

CONCLUSION: Our data showed that non-working heart allograft hearts had very poor cardiac functions and rejected much faster than the working heart models, even though they both showed strong palpation and normal ECG, which is not adequate for complementary graft evaluation. With our working heart model, cellular and functional MRI can repeatedly evaluate rejection and function status of the graft hearts in real time with whole heart information and avoid biases during investigation of the immune response.

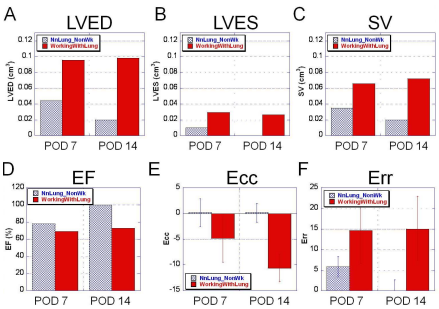

Figure 1 Cardiac function of both the non-working heart model (blue grids) and the working heart model (red filled) at post-operational-day (POD) 7 and 14. (A) left-ventricular (LV) volume at the end-diastole (LVED); (B) LV volume at the end-systole (LVES); (C) stroke volume (SV); (D) ejection fraction (EF); (E) circumferential strain (Ecc); and (F) radial strain (Err).

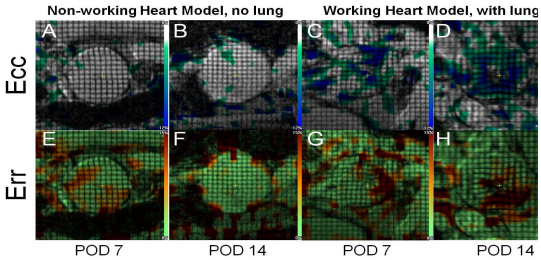

Figure 2 Circumferential strain (Ecc) maps (A-D) and radial strain (Err) maps (E-H) generated from tagging MRI for both the non-working heart model (A, B, E, F) and the working heart model (C, D, G, H).

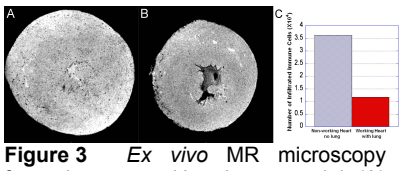

Figure 3 *Ex vivo* MR microscopy from the nonworking heart model (A) and the working heart model (B) after *in vivo* MPIO labeling harvest on POD 15. (C) Quantitation of all infiltrated cells detected for the non-working heart model (blue grids) and the working heart model (red filled).

REFERENCES:

1. Martins PN. Microsurgery. 2008;28(7):565-70.
2. Ye Q, Wu YL, Foley LM., et al. Circulation. 2008 Jul 8;118(2):149-56.
3. Wu YL, Ye Q, Sato K., et al. JACC Cardiovasc Imaging. 2009 Jun;2(6):731-41.

ACKNOWLEDGMENTS: This work was supported by grants from the National Institutes of Health (P41EB001977 and R01HL-081349)